REVIEWS

Journal of Semiconductors
(2020) 41, 091707
doi: 10.1088/1674-4926/41/9/091707

Metal-organic framework composites for energy conversion and storage

Hang Wang[1], Na Zhang[1], Shumin Li[2], Qinfei Ke[1, †], Zhengquan Li[2, †], and Min Zhou[3, †]

[1]School of Materials Science and Engineering, Shanghai Institute of Technology, Shanghai 201418, China

[2]Key Laboratory of the Ministry of Education for Advanced Catalysis Materials, Zhejiang Normal University, Jinhua 321004, China

[3]Hefei National Laboratory for Physical Sciences at the Microscale, School of Chemistry and Materials Science, University of Science and Technology of China, Hefei 230026, China

Abstract: Metal-organic frameworks (MOFs) with orderly porous structure, large surface area, high electrochemical response and chemical tunability have been widely studied for energy conversion and storage. However, most reported MOFs still suffer from poor stability, insufficient conductivity, and low utilization of active sites. One strategy to circumvent these issues is to optimize MOFs via designing composites. Here, the design principle from the viewpoint of the intrinsic relationships among various components will be illuminated to acquire the synergistic effects, including two working modes: (1) MOFs with assistant components, (2) MOFs with other function components. This review introduces recent research progress of MOF-based composites with their typical applications in energy conversion (catalysis) and storage (supercapacitor and ion battery). Finally, the challenges and future prospects of MOF-based composites will be discussed in terms of maximizing composite properties.

Key words: metal-organic frameworks; composites; synergistic effect; energy conversion; energy storage

Citation: H Wang, N Zhang, S M Li, Q F Ke, Z Q Li, and M Zhou, Metal-organic framework composites for energy conversion and storage[J]. *J. Semicond.*, 2020, 41(9), 091707. http://doi.org/10.1088/1674-4926/41/9/091707

1. Introduction

With dramatical growth of the global energy demand and consumption, there is a urgent need to utilize clean and renewable energy resources, such as solar energy[1–3]. Yet these resources are intermittent and strongly related to weather and environment. Thus it is vital to develop efficient technologies associated with energy conversion and storage to convert these resources into usable electricity[4]. Among the energy conversion systems, catalysis used for fuel production and water oxidation, such as photochemical or electrochemical H_2 production and CO_2 reduction, are efficient ways to convert solar energy into chemical energy[5]. Additionally, supercapacitors and ion batteries that can store chemical energy to electricity have been regarded as promising energy storage devices for large-scale applications[6, 7]. Energy conversion and storage devices with high efficiency and excellent stability have attracted intensive attention from both fundamental research and industry fields[8]. Since the similar construction within these devices, materials used as electrodes and separators are basic stone. Designing suitable materials are facing challenges.

Among the emerging materials, metal-organic frameworks (MOFs) have gained considerable attention and exhibited remarkable superiorities over the conventional materials for energy conversion and storage[9]. MOFs are generally constructed via self-assembling metal ions and organic ligands[10]. However, most reported MOFs still suffer from poor stability, insufficient conductivity, and low utilization of active sites[11]. Thus, the full utilization of MOFs is somewhat hindered for practical applications. With the increased requirements of highly efficient energy conversion and storage devices, a single material is insufficient for complex functions. The overall performance of MOF-based composites is expected to achieve further improvements based on the synergistic effects by integrating the advantages of different components.

Considering that properties of composites are mainly related to the kinds of components and the interconnections among separated components, the fundamental principle of construction is vital for MOF-based composites. As shown in Scheme 1, MOF-based composites can be generally divided into two strategies according to the working modes during energy conversion and storage processes: (1) MOFs with assistant components, (2) MOFs with other function components. For the former one, MOFs possess the main functions within the composites, while the other components will not directly participate the energy conversion and storage, but can assist MOFs for full utilizations by adjusting related properties; as for the latter one, MOFs and the other components all join in energy conversion and storage simultaneously.

In this review, we present a deep discussion on the design principle of MOF-based composites from the viewpoint of the intrinsic relationships among various components. Then, MOF-based composites for energy conversion and storage, such as catalysis[12], supercapacitor[13] and ion battery[14], will be illustrated respectively to testify the superiorities of MOF-based composites with the two working modes. Finally, the challenges and perspectives of MOF-based composites are provided in terms of maximizing their applications for

Correspondence to: Q F Ke, kqf@shnu.edu.cn; Z Q Li, zqli@zjnu.edu.cn; M Zhou, mzchem@ustc.edu.cn
Received 7 JULY 2020; Revised 3 AUGUST 2020.

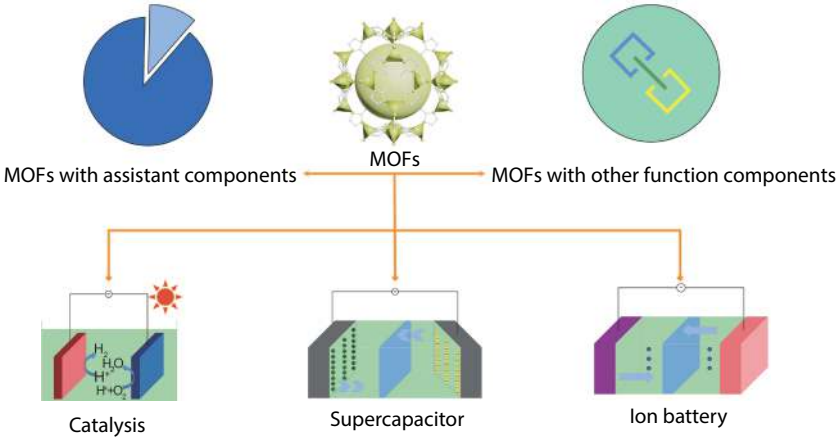

Scheme 1. (Color online) Design principle of MOF-based composites.

energy conversion and storage.

2. Design principle of MOF-based composites

Tracing the previous progress, we focus on the progress of MOF-based composites in catalysis, supercapacitor and ion battery. According to relationships among various components within composites, MOF-based composites can be classified into two working modes in Scheme 1: MOFs with assistant components and MOFs with other function components.

The design of MOF-based composites with assistant components is a design strategy where the performance of MOFs is reinforced by the secondary component to improve the overall performance. In the composites, MOFs play a dominant role, and the other component has auxiliary effect which is denoted as assistant components. And the assistant components do not directly join all the physical process and chemical reactions of energy conversion and storage. For instance, the photosensitized mechanism to extend the absorption of photons can achieve wide spectral response[15]. Through light harvesting of photosensitive components, more solar energy was utilized by MOFs to produce photo-generated carriers. On the other hand, combining MOFs with conductive materials can facilitate the transfer of electrons for energy storage[16]. High carrier migration efficiency due to conductive materials would be efficient to solve the problems originated from poor conductivity of MOFs.

So as to the second working mode of MOFs composites, the other function components is designed to achieve cooperative effects, where the improvements of comprehensive performance is attributed to the comprehensive actions of different components. Generally, each component remains the capability of energy conversion or storage and directly participates in the related steps while improving performance in the composites. For example, regulating electronic states of noble metal/MOF composites is able to facilitate charge separation and transfer to improve performance for energy conversion[17]. It can improve light absorption by sensitizing MOFs with wide bandgap based on injecting hot electrons/hot holes into MOFs. On the other hand, cross Schottky barrier from MOFs to plasma can promote the charge separation process. In addition, the optimization of the effective active sites was a method to enhanced charge transfer kinetics and ensure high charge storage capability[18]. The synergistic effects between different components can not only remain the capacity of each components, but also shortened diffusion paths for charge transfer and facilitated the fast transport of ions to realize extra energy storage.

Such a design principle, which can acquire the synergistic effects based on integration the advantages of different components, will contribute to illuminate the correlations between the intrinsic relationships of different components and properties of energy conversion and storage. And the further instructions will be elaborated in the following sections using the detailed application of energy conversion and storage.

3. MOFs with assistant components

3.1. Catalysis

According to the energy source of catalytic reactions, catalysis can be divided into photocatalysis, electrocatalysis, photoelectrocatalysis and so on[1, 5, 19]. MOFs are considered as promising catalysts due to their functional surface groups and the adjustable band structure[20]. However, they are still limited in some shortcomings, such as low energy utilization efficiency. Herein, there are three main aspects results from the assistant components, including light absorption, separation/migration of charge and surface reactions, which can promote the development and practical applications of MOFs for energy conversion. As shown in Table 1, MOFs undertake the main tasks of catalysis, while related properties can be adjusted by assistant components to enhance overall performance.

Light harvesting is the first step of photocatalysis or photoelectrocatalysis, which determines the basis for the subsequent energy conversion. Thus, one of the limitations to increase the efficiency of energy conversion process is insufficient photo-response to visible light or the unsatisfactory activity under solar-light exposure. This downside of MOFs can be ameliorated with the assistant components such as dye and upconversion materials[15, 21, 22]. In the composite system, both photosensitized materials and MOFs synergistically work together as the light harvesting and catalytic sites, respectively. Li and co-workers[21] reported that three yellow/red/blue cationic dyes were successfully assembled into an identical MOF host singly, dually, and triply (Figs. 1(a) and 1(b)). Improvement of absorption band range and absorbance intensities for multi-dye@MOF composites could be observed via UV–vis DRS. And the E_g value (1.72 eV) was far nar-

Table 1. MOF-based compositions for catalysis.

	Material	MOF	Assistant species	Influence	Ref.
1	UiO-66/Erythrosin B	UiO-66	Erythrosin B	Enhance photon utilization	[15]
2	cationic-dye@MOF	In-MOF	cationic dye	Enhance photon utilization	[21]
3	$NaYF_4$:Yb,Tm/NH_2-MIL-53(Fe)	NH_2-MIL-53(Fe)	$NaYF_4$:Yb,Tm	Enhance photon utilization	[22]
4	MIL-88A(Fe)/GO	MIL-88A(Fe)	GO	Facilitate carrier separation	[23]
5	CD@NH_2-UiO-66	NH_2-UiO-66	CD	Facilitate carrier separation	[24]
6	G-dye/Fe-MOF	Fe-MOF	G-dye	Facilitate electron mobility	[25]
7	Co-MOF@CNTs	Co-MOF	CNTs	Facilitate electron mobility	[26]
8	ZIF-67@HMCS	ZIF-67	HMCS	Facilitate electron mobility	[27]
9	Fe-UiO-66	UiO-66	FeO_x	Accelerate surface reaction	[28]
9	$CoFeO_x$/Co-MOF	Co-MOF	$CoFeO_x$	Accelerate surface reaction	[29]
10	MOF-525-Co	MOF-525	Co	Accelerate surface reaction	[30]

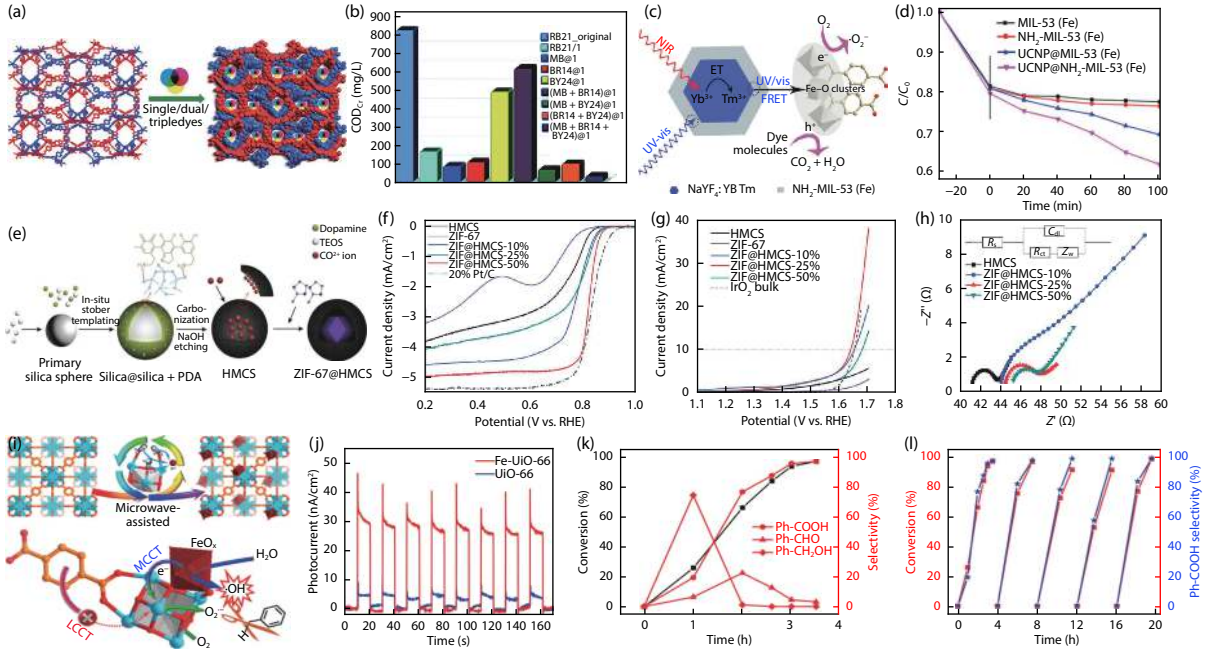

Fig. 1. (Color online) Typical examples of MOFs with assistance components for catalysis. (a) Schematic illustration of the cationic-dye@MOF. (b) The COD_{Cr} changes of RB21 before and after visible-light irradiation in the presence of several composite photocatalysts[21]. Copyright 2018, Royal Society of Chemistry. (c) Schematic illustration of the photocatalytic mechanism of the prepared composites. (d) Degradation profiles of RhB solution of samples activities under the NIR light[22]. Copyright 2017, American Chemical Society. (e) Schematic illustration of synthetic procedure for ZIF@HMCS. (f) The linear scan voltammogram (LSV) curves toward ORR of various samples. (g) LSV curves toward OER of various samples. (h) High frequency range electrochemical impedance spectroscopy (EIS) after fitting of various samples (inset: the corresponding equivalent circuit diagram)[27]. Copyright 2019, Oxford University Press. (i) Schematic illustration of Fe-UiO-66 and activation of stubborn C–H bond under visible light irradiation. (j) Photocurrent signals of UiO-66 and Fe-UiO-66. (k) Conversion/Selectivity-Time plot of toluene oxidation over Fe-UiO-66 under visible light irradiation. (l) Recycling tests of toluene oxidation over Fe-UiO-66 under optimized reaction conditions[28]. Copyright 2019, American Chemical Society.

rower than that of bare MOF (2.87 eV). The composites could improve the light utilization efficiency by the incorporation of photosensitive components into MOFs, exhibiting the superior performance compared with the commercial TiO_2. Besides, integrating upconversion materials with MOFs will be a good choice to further broaden the light absorption range. And it will be able to utilize both UV-visible and near-infrared (NIR) lights due to the MOF photocatalysts can be activated by UV/visible photons. Li and co-workers proposed a facile approach to integrate $NaYF_4$:Yb, Tm with NH_2-MIL-53(Fe) to build a NIR-responsive composite photocatalyst[22]. The upconversion materials would not directly join in photocatalytic reactions, but could enhance near-infrared light harvesting (Figs. 1(c) and 1(d)). Specifically, the main absorption of NH_2-MIL-53(Fe) is in the range of 200–700 nm. After modification with UCNP, the absorption of the composites have been significantly enhanced, and the absorption edge was extended to 1100 nm.

Additionally, electron–hole recombination associated with low internal charge separation efficiency of MOFs becomes the key issues of limitation of energy conversion efficiency. And the most organic ligands used for MOFs synthesis do not facilitate electron transfer. The introduction of conductive additives, such as metal, carbon materials, can contribute to carrier separation for photocatalysis or photoelectrocatalysis, leading to suppressing carrier recombination[23, 24]. On the other hand, this strategy can be used to reduce the charge transfer barrier and facilitate charge mobi-

Table 2. MOF-based compositions for supercapacitor.

	Material	MOF	Assistant species	Influence	Ref.
1	Na-Zn-MOF/rGO	Na/Zn-MOF	rGO	Boost charge transfer	[33]
2	Ni-MOF@GO	Ni-MOF	GO	Boost charge transfer	[34]
3	Ni-MOF/CNT	Ni-MOF	CNT	Boost charge transfer	[35]
4	CoNi-MOF/CFP	CoNi-MOF	CFP	Increasing stability	[36]
5	CNF@Ni-MOF	Ni-MOF	CNF	Improving flexibility	[37]
6	PPNF@MOF	MOF	PPNF	Increasing stability	[38]

lity[25–27]. Liu and co-workers[23] presented the MIL-88A/graphene oxide composites for photocatalysis via polymerizing the ultrathin graphene oxides on the surface of the MIL-88A. The presence of graphene oxide could improve electrical conductivity. And the intimate interface of MIL-88A and graphene oxide provided a conductive path in short distance to facilitate carriers separation and avoid recombination of photogenerated electron–hole. Additionally, Xiong and colleagues[27] proposed the synthesis of ZIF-67@hollow mesoporous carbon spheres (HMCS) via a facile in-situ growth method to improve the electrochemical activity for electrocatalysis (Fig. 1(e)). In this composite, HMCS increased electrical conductivity and shortened the diffusion paths to facilitate electron mobility. It could be clearly seen from the electrochemical data (Figs. 1(f)–1(h)) that the ZIF@HMCS-25% showed a highly efficient oxygen reduction reaction activity than commercial Pt/C, and excellent oxygen evolution reaction performance compared with IrO_2.

In addition, surface reaction rates have also been regarded as another limitation in catalysis[28–30]. Modulating the electronic structure and configuration by changing the surrounding chemical environment of MOFs can optimize reaction intermediate energies and decrease reaction barriers. It should be stated that the assistant components to MOFs serve more likely as electron donors to change the required activation energy of catalysis reactions on the surface of MOFs, instead of electron mediators. And assistant components will not directly take part in the catalysis reactions. Fig. 1(i) showed a typical example about grafting FeO_x onto the UiO-66 to afford Fe-UiO-66[28]. The FeO_x to M-oxo clusters herein altered the surface coordination environment to reduce the activation energy. Thus the Fe-UiO-66 achieved fast surface reactions to activate "inert" MOFs for photocatalysis. The results showed the Fe-UiO-66 displayed 70.1% toluene conversion in the first 2 h and finally 96.9% conversion with nearly complete selectivity to benzoic acid at 3.5 h. It indicated that the Fe-UiO-66 displayed visible light-driven water oxidation and cycling stability, which was impossible for pristine UiO-66 (Figs. 1(j)–1(l)). Moreover, Zhang and co-workers proposed the $CoFeO_x$/Co-MOF as a promising OER electrocatalyst[29]. The interfacial Co possessed a higher valence and changed 3d electronic configuration compared to the CoN_4 sites of pure Co-MOF. Moreover, it showed excellent electrocatalytic performance with a low overpotential of 232 mV at a current density of 10 mA/cm^2. Besides, constructing single-atom catalysts on MOFs is a research focus due to the involvement of the strong metal-support interactions arising from interfacial bonding based on the presence of single atoms. And it will contribute to accelerate surface reaction rates. Zhang and co-workers[30] revealed the introduction of single Co atoms within the MOF. The involvement of single atoms could supply long-lived electrons to active CO_2 molecules that were adsorbed on Co centers. Thus, the MOF-525-Co significantly enhanced photocatalytic conversion of CO_2, which was equivalent to a 3.13-fold enhancement in CO generationration (200.6 mmol g^{-1} h^{-1}) and a 5.93-fold improvement in CH_4 evolution rate (36.67 mmol g^{-1} h^{-1}) in contrast to the pristine MOFs.

3.2. Supercapacitor

Among various energy storage devices, supercapacitors have been widely studied owing to their fast charging/discharging, high power density and long cycle life[2, 3]. The energy storage mechanism of supercapacitors can be generally classified into two categories: electric double layer capacitance and pseudocapacitance. Currently, the MOFs-based electrode materials have become the research focus of supercapacitors[31, 32]. Up to now, typical MOF composites used for supercapacitors are briefly summarized in Table 2. And they will be clarified through the functions of the other components into three types, boosting charge transfer, improving flexibility and increasing stability.

Pristine MOFs with poor conductivity always have limited electrochemical performance. In order to full achieve the theoretical capacity of active materials, researchers have tried to introduce conductive materials as assistant components, such as carbon, metals materials[33–35]. And the synergy of the high electrical conductivity from assistant components and capacitance property from MOFs can reduce the charge transfer barrier of MOFs to facilitate charge transfer. Conductive materials can serve as a current collector to accelerate charge collection and shorten the charge transfer paths. Binary metal-organic framework/reduced graphene oxide (Na-Zn-MOF/rGO) is a typical instance (Fig. 2(a))[33]. As shown in Figs. 2(b)–2(d), the composites showed the specific capacitance of 435.2 F/g at 1.6 A/g, and stable cycling efficiency (no observed loss up to 4000 cycles in the absence of any binders). The significantly improved performance was attributed to the introduction of layered structures of rGO and followingly fast charge migration. In addition, Wen and co-workers[35] successfully synthesized nickel metal-organic framework/carbon nanotube (Ni-MOF/CNT) to improve the conductivity of MOFs achieving a specific capacitance of 1765 F/g at a current density of 0.5 A/g. Moreover, this asymmetric supercapacitor revealed a cycle life along with 95% specific capacitance retention after 5000 consecutive charge-discharge tests.

So far, various conductive MOFs have been reported by linking fully conjugated organic linkers to improve electrochemical performance[32]. However, inevitable disadvantages of MOFs like flexibility, limit their practical applications for energy-storage devices powering flexible electronics. It can construct flexible supercapacitor with high mechanical and chem-

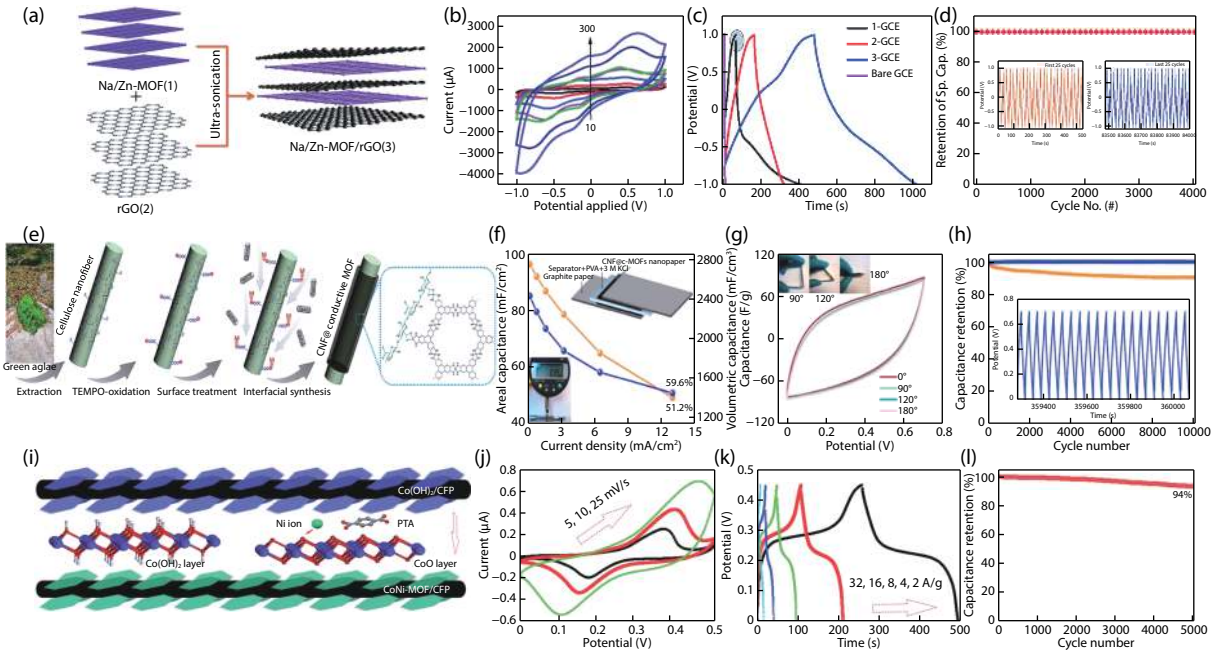

Fig. 2. (Color online) Typical examples of MOFs with assistance components for supercapacitor. (a) Schematic diagram of Na-Zn-MOF/rGO. (b) The cyclic voltammograms (CV) collected of Na-Zn-MOF/rGO electrode. (c) A comparison of the GCD curves of a bare GCE, 1-GCE, 2-GCE and 3-GCE. (d) Cycling stability analysis of Na-Zn-MOF/rGO over 4000 cycles(the left and right insets show the first and last 25 cycles)[33]. Copyright 2019, Royal Society of Chemistry. (e) Schematic of synthesis procedure for CNF@MOF hybrid nanofibers. (f) Calculated areal capacitances of the device at different current densities within 0–0.7 V (blue curve) and 0–1.0 V (orange curve). (g) The CV curves at scan rate of 100 mV/s under different folding angles. (h) Cyclic performance and capacitance retention data of the device within 0–0.7 V (blue curve) and 0–1.0 V (orange curve)[36]. Copyright 2019, Wiley-VCH Verlag GmbH & Co. KGaA. (i) The schematic illustration of the strategy to synthesize CoNi-MOF/CFP. (j) CV curves of CoNi-MOF at a scan rate of 5, 10, and 25 mV/s. (k) Galvanostatic curves collected at a current density of 2, 4, 8, 16, and 32 A/g. (l) The cyclability of the capacitor over 5000 cycles[37]. Copyright 2019, American Chemical Society.

ical stability by introducing flexible substrate material to improve performance of MOFs. Fig. 2(e) exhibited the schematic of the fabrication of conductive Ni-MOF nanolayers on cellulose nanofibers (CNFs) with formation of CNF@Ni-MOF by interfacial synthesis[36]. Bending (90°, 120°) or even folding (180°) the device of CNF@Ni-MOF had no influence on the CV curves. This work would not only warrant high flexibility of the nanocomposites, but also increase the electrochemical performance of the composites via uniform distribution of MOFs at the surface of CNF (Figs. 2(f)–2(h)).

Besides, stability is one of the most essential parameter for supercapacitor[37, 38]. The plugging of porous channels and the large volume change of MOFs in long-term cycling will decrease surface area to reduced cyclic stability. And it is difficult for MOF crystals to control morphology/alignment and avert aggregation. The preventive strategy is to introduce the inner scaffold to provide the in-situ growing platform. Fig. 2(i) showed that a novel method to fabricate vertically-oriented MOF electrode on the surface of carbon fiber paper (CFP) was proposed by Deng and co-workers[37]. The presence of CFP could suppress aggregation and ensure high loading of CoNi-MOF simultaneously to enhance stability. As a direct return, the CoNi-MOF/CFP electrode displayed quite satisfied electrochemical performance (Figs. 2(j)–2(k)). The electrode showed a double high specific capacitance of 1044 F/g and great cyclability by delivering 94% specific capacitance retention after 5000 cycles (Fig. 2(l)).

3.3. Ion battery

Generally, ion batteries like Li ion battery, Na ion battery and K ion battery, etc., have higher energy density compared with supercapacitors, but their lower power density is insufficient for practical applications[7, 14, 39]. To date, MOFs composites have utilized for ion batteries on account of their large surface area, high electrochemical response, and superior theoretical ions storage capacity. And typical MOF-based composites as electrodes and separators of ion battery are summarized in Table 3. The rationale behind design always centers on enhancing ions migration as well as improving processability and stability.

MOF-based electrodes usually exhibit poor rate capacities owing to their low conductivity. Moreover, the high surface area and porosity of MOF materials may lead to low initial Coulombic efficiency and low tap density. Combining MOFs with conductive agents such as carbon materials, conducting polymer and metal materials, has been used to circumvent these issues[16, 40–44]. Continuous conductive pathways provide the efficient skeleton to fasten electron movement, especially at high rates where electrons are generated in a short interval. As shown in the Figs. 3(a) and 3(b), Al-MOF/graphene composite was synthesized via a facile self-assembly method by Gao and colleagues[40]. These graphene sheets with high electronic conductivity could boost the charge transfer and simultaneously provide a new path for the Li^+ ions migration during the lithiation/delithiation. The work exhibited a drastic increase in specific capacity from 60 to 400 mAh/g at the current density of 100 mA/g with increased discharging/charging cycles (Figs. 3(c) and 3(d)). For Li–S battery, Mao and co-workers presented a MOFs/CNT thin

Table 3. The MOF-based compositions for ion battery.

	Material	MOF	Assistant species	Influence	Application	Ref.
1	Al-MOF/GO	Al-MOF	GO	Enhance ions migration	Anode	[40]
2	POMOF/rGO	POMOF	rGO	Enhance ions migration	Anode	[41]
3	MOF-74/super P	MOF-74	Super P	Enhance ions migration	Cathode	[16]
4	MIL-100/rGO	MIL-100	rGO	Enhance ions migration	Cathode	[42]
5	MOF@CNT	MOF	CNT	Enhance ions migration	Cathode	[43]
6	PPy-PCN-224	PCN-224	PPy	Enhance ions migration	Cathode	[39]
7	ZIF-8@CNT	ZIF-8	CNT	Enhance ions migration	Cathode	[44]
8	$Ni_3(HITP)_2$/PP	$Ni_3(HITP)_2$	PP	Improve processability and stability	Separator	[45]
9	HKUST-1@PVDF-HFP	HKUST-1	PVDF-HFP	Improve processability and stability	Separator	[46]
10	UiO-66/PVA	UiO-66	PVA	Improve processability and stability	Separator	[47]

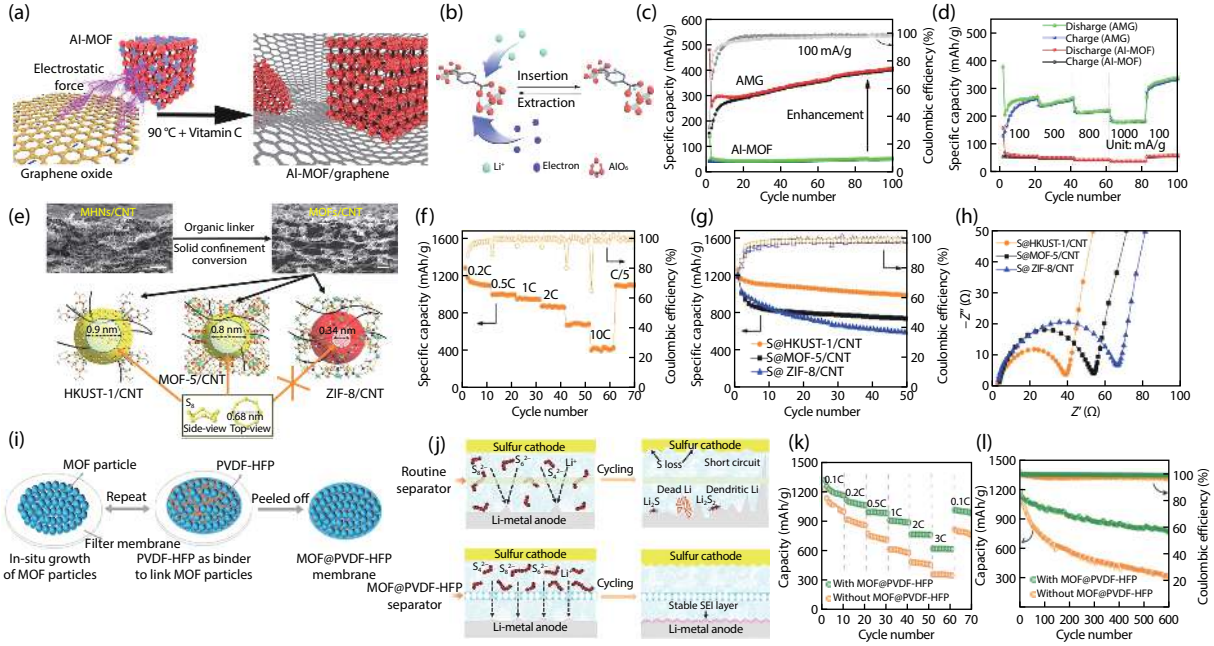

Fig. 3. (Color online) Typical examples of MOFs with assistance components for ion battery. (a) Schematic representation of the preparation process of Al-MOF/GO composite. (b) Proposed Li^+ ions insertion-extraction process into or from Al-MOF. (c) Cycling performance and coulombic efficiency of Al-MOF and AMG at a current density of 100 mA/g. (d) The rate capability of Al-MOF and AMG[40]. Copyright 2019, Elsevier. (e) Synthesis of MOFs/CNT composite thin films. (f) The rate performances of S@HKUST-1/CNT electrode. (g) The cycling performances of S@HKUST-1/CNT, S@MOF-5/CNT and S@ZIF-8/CNT electrodes, respectively. (h) Nyquist plots of S@HKUST-1/CNT, S@MOF-5/CNT and S@ZIF-8/CNT electrodes, respectively[43]. Copyright 2017, Springer Nature. (i) Schematic illustration for fabricating a flexible MOF@PVDF-HFP membrane. (j) Schematic for Li-S batteries with different separators with a routine separator and MOF@PVDF-HFP separator. (k) The rate performance of Li–S cells with and without MOF@PVDF-HFP separators. (l) Comparison of the cycling performance of Li–S cells with and without MOF@PVDF-HFP separators[46]. Copyright 2018, Wiley-VCH Verlag GmbH & Co. KGaA.

film[43]. As presented in Fig. 3(e), the CNTs interpenetrated with the MOFs crystals and interweaved the electrode into a stratified structure to design the hierarchical porous structure and three-dimensional conductive networks. The design demonstrated great cycling stability for 500 cycles with 0.08% decay per cycle and high volumetric energy density of 1195 mAh/cm^3 (Figs. 3(f)–3(h)).

In addition, the open metal sites in the MOFs provide an effective route to modulate the transport of ions as separators[45–47]. However, due to the intrinsic mechanical brittleness of MOFs, it is difficult to fabricate an ideal ionic sieve membrane. The MOFs grown in situ on the polymer matrix to improve processability can suppress the aggregation of MOFs. Thus it can retain the ordered microporous structure and large specific surface area to transfer ions. On the other hand, polymer matrix can also efficiently prevent volume expansion and contraction during ions intercalation or deintercalation to achieve the high cycling stability. Fig. 3(i) showed the copper metal-organic framework/poly vinylidenefluoride-hexafluoro propylene (HKUST-1@PVDF-HFP) with good processability by a facial vacuum filtration strategy[46]. With a routine separator, the soluble intermediate polysulfide species formed from sulfur cathode could pass through the separator to Li anode and react with the Li-metal to produce insoluble Li_2S and Li_2S_2 on the surface of anode, resulting in surface passivation of Li anode (Fig. 3(j)). Correspondingly, the uniformly ordered pores with around 9 Å pore sizes were generated from PVDF-HFP. As a Li–S battery of separator of MOF@PVDF-HFP, a cycle life with an ultralow capacity fading could be realized upon 2000 cycles (0.013% per cycle) (Figs. 3(k) and 3(l)), and it exhibited decent processability and stability with different bended shapes.

Table 4. The component of the MOF-based compositions for catalysis.

	Material	MOF	Function species	Ref.
1	NH_2-MIL-68@TPA-COF	NH_2-MIL-68	TPA-COF	[5]
2	NH_2-UiO-66/TpPa-1-COF	NH_2-UiO-66	TpPa-1-COF	[48]
3	CdS/Ni-MOF	Ni-MOF	CdS	[49]
4	UiO-66/CNNS	UiO-6	CNNS	[50]
5	$CsPbBr_3$@ZIF	ZIF	$CsPbBr_3$	[51]
6	$MAPbI_3$@PCN-221	PCN-221	$MAPbI_3$	[52]
7	Pt/PCN-224	PCN-224	Pt	[17]
8	Pt/Al-TCPP	Al-TCPP	Pt	[53]
9	Pt@2D MOFs	2D MOFs	Pt	[54]
10	Ni-MOF@Pt	Ni-MOF	Pt	[55]
11	$Ti_3C_2T_x$-CoBDC	CoBDC	$Ti_3C_2T_x$	[56]
12	CoP/Co-MOF	Co-MOF	CoP	[57]

4. MOFs with other function components

4.1. Catalysis

With regard to 'MOFs with other function components', the other function components hold the ability of catalysis like MOFs. Meanwhile, the incorporation of different function components can achieve synergetic effect as shown in Table 4. The design principle, including band engineering, surface plasmon resonance (SPR) effect and surface reaction, will be illuminated as following.

For photocatalysis or photoelectrocatalysis, light absorption range can also be adjusted by band engineering for large light harvesting[5, 48–52]. MOFs with wide bandgap can combine with a component with relatively narrow bandgap to absorb photons of higher energies and improve the harvesting of visible light. Besides, it can form a heterojunction to produce strong electric fields at the interface between MOFs and the other functional components, leading to more efficient electron–hole separation. So a promising approach is to combine MOFs with other semiconductor materials such as covalent organic frameworks (COFs), transition metal sulfides, perovskites and so on. The MOF/COF hybrid materials by covalently anchoring NH_2-UiO-66 onto the surface of TpPa-1-COF as shown in the Fig. 4(a), were synthesized by Zhang's group[48]. The NH_2-UiO-66/TpPa-1-COF showed the maximum photocatalytic H_2 evolution rate of 23.41 mmol g^{-1} h^{-1} under visible light irradiation (Figs. 4(b) and 4(c)). NH_2-UiO-66 exhibited the optical absorbance with the edge at 440 nm (2.88 eV), while the absorbance of TpPa-1-COF can even cover the whole UV/Vis region with a broadly intense absorbance below 600 nm (2.02 eV) as shown in Fig. 4(d). Due to the introduction of TpPa-1-COF the composites could broaden the light absorption range compared to the pure NH_2-UiO-66. In addition, due to the heterojunction between the NH_2-UiO-66 and TpPa-1-COF ensured the separation and transfer of photogenerated electrons and holes. The photogenerated electrons of TpPa-1-COF migrated from valence band (VB) to conduction band (CB), which would further transfer to the CB of NH_2-UiO-66 through covalent connecting junction. Besides, Wu and co-workers[52] encapsulated low-cost $CH_3NH_3PbI_3$ ($MAPbI_3$) perovskite quantum dots in the pores of earth-abundant Fe-porphyrin based PCN-221. And the schematic illustration for the synthesis of $MAPbI_3$@PCN-221(Fe_x) was shown in Fig. 4(e). The composite photocatalysts exhibited significantly enhanced yields for CO_2 reduction, 25–38 times higher than the corresponding PCN-221(Fe_x) without perovskite quantum dots (Fig. 4(f)). And it could promote carrier separation, and electrons could transfer rapidly from $MAPbI_3$ to PCN-221 (Figs. 4(g) and 4(h)).

Another solution based on SPR effect, such as the integration of noble metal into MOFs, is another effective way to accelerate photocatalysis or photoelectrocatalysis reaction[17, 53–55]. Plasmonic components can not only directly take part in the reactions of catalysis, but also contribute on resonant photon-induced collective oscillation of valence electrons. On the one hand, the introduction of SPR effect can sensitize wide-bandgap MOFs by injecting hot electrons/hot holes into MOFs to improve light absorption. On the other hand, it is possible to cross Schottky barrier from MOFs to plasma to trap electrons from MOFs, and thus promote the charge separation process and mitigate the electron–hole recombination. Fang and colleagues[53] explored that single Pt atoms were successfully confined into Al-MOF(denoted as Al-TCPP). And electrons could transfer from MOF to Pt for hydrogen production under visible-light irradiation as shown in Fig. 4(i). This work exhibited a much higher photocatalytic H_2 production rate of 50 μmol g^{-1} h^{-1} and no noticeable change in the H_2 production rate during the four runs (Figs. 4(j) and 4(k)). Highly efficient H_2 production of the composites could mainly be attributed to the surface plasma resonance effect of Pt nanoparticles, which could enhance photon absorption and promote the carriers separation (Fig. 4(l)). In addition, Rui and co-workers[55] explored a surfactant-free approach to realize in-situ growth of Pt nanoparticles on MOF nanosheets, denoted as Ni-MOF@Pt, for the electrochemical H_2 evolution reaction. Their work indicated the incorporation of highly dispersed noble metal nanoparticles exhibited excellent electrocatalytic activity under both acidic and alkaline conditions.

Additionally, MOF with other function components can also facilitate surface reactions via the synergy of multiple active sites, which can increase the lifetime of the electrons by many orders of magnitude in catalysis[56, 57]. First, the function components can contribute to capacity of catalysis based on the intrinsic electrochemical activity. Second, the direct contact between MOFs and other function components enables the creation of new interfaces, which are associating with the reduction of required activation energy of catalysis reaction. Fig. 4(m) showed the synthesis hybridized CoBDC with $Ti_3C_2T_x$ nanosheets via an interdiffusion reaction-assisted process[56]. The presence of electrically conductive and hydrophilic $Ti_3C_2T_x$ nanosheets changed the coordination environment of metal center atoms of CoBDC. The study indicated that the composites reduced the charge transfer barrier across the interface between $Ti_3C_2T_x$ and CoBDC. And it could be clearly seen from the electrochemical data (Figs. 4(n)–4(p)) that the $Ti_3C_2T_x$-CoBDC contributed to the high OER activity than commercial IrO_2. Besides, Liu and co-workers[57] reported a controllable partial phosphorization strategy to generate CoP species within the Co-MOF. The electron transfer through N-P/N-Co bonds could lead to the optimized adsorption energy of H_2O and hydrogen based on density functional theory calculations. And the CoP/Co-MOF achieved the re-

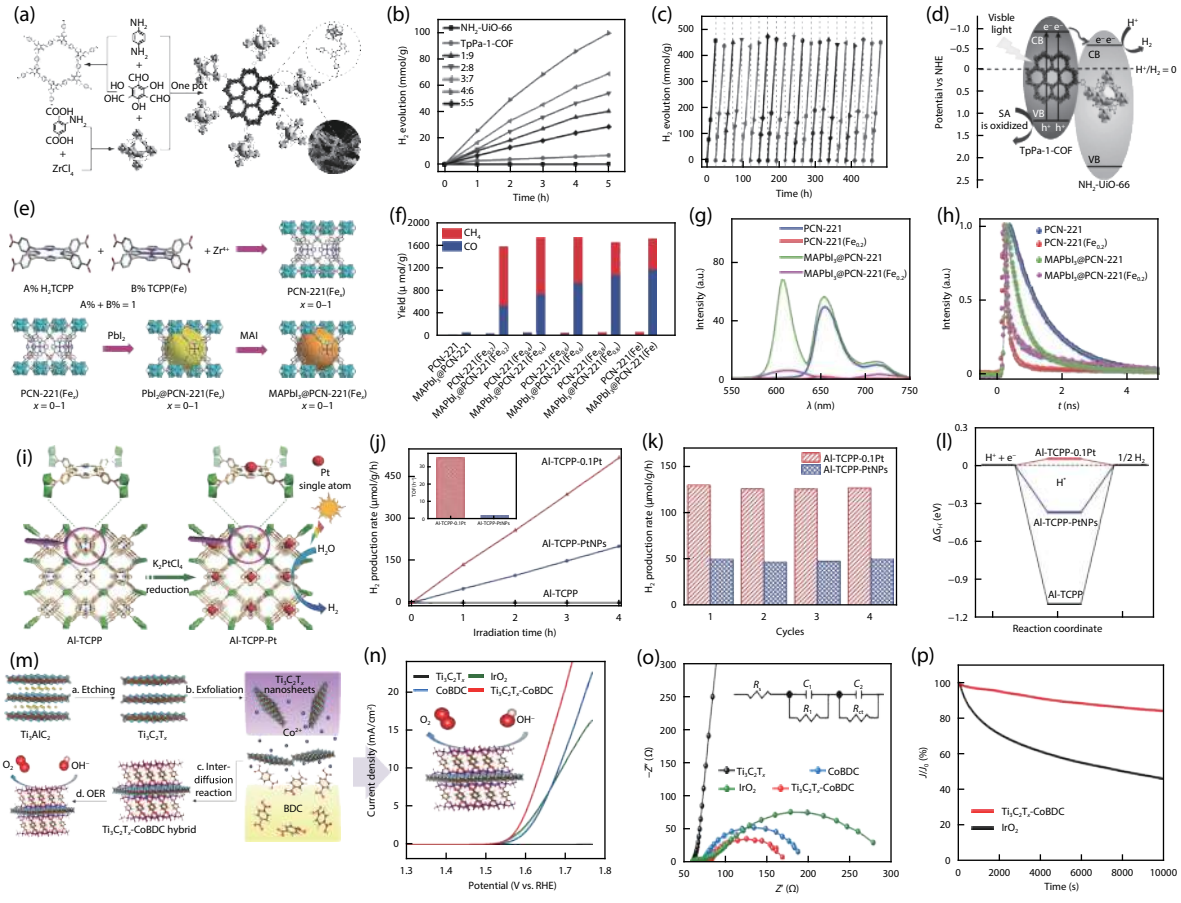

Fig. 4. (Color online) Typical examples of MOFs with function components for catalysis. (a) Schematic illustration of the synthesis of NH_2-UiO-66/TpPa-1-COF hybrid material. (b) The photocatalytic H_2 evolution activities. (c) The photocatalytic stability of NH_2-UiO-66/TpPa-1-COF (4 : 6). (d) Mechanism schematic of NH_2-UiO-66/TpPa-1-COF (4 : 6) hybrid material[48]. Copyright 2018, Wiley-VCH Verlag GmbH & Co. KGaA. (e) Schematic illustrations for the synthesis of $MAPbI_3$@PCN-221. (f) The yields for CO_2 reduction to CH_4 and CO with PCN-221 and $MAPbI_3$@PCN-221 as photocatalysts in the CO_2-saturated ethyl acetate/water solution. (g) Steady-state photoluminescence spectra of various samples. (h) Time-resolved photoluminescence decays of various samples[52]. Copyright 2019, Wiley-VCH Verlag GmbH & Co. KGaA. (i) Schematic illustration showing the synthesis of Al-TCPP-Pt for photocatalytic hydrogen production. (j) Photocatalytic hydrogen production rates of various samples (inset: the calculated turnover frequency (TOF) of Al-TCPP-PtNPs and Al-TCPP-0.1Pt). (k) Recycling performance comparison for Al-TCPP-PtNPs and Al-TCPP-0.1Pt. (l) Calculated free energy diagram for photocatalytic H_2 production[53]. Copyright 2018, Wiley-VCH Verlag GmbH & Co. KGaA. (m) Schematic illustration of the synthesis process of $Ti_3C_2T_x$-CoBDC hybrid for oxygen evolution reaction. (n) OER polarization curves of various electrodes. (o) Nyquist plots of the electrodes modified by IrO_2, $Ti_3C_2T_x$, CoBDC, and $Ti_3C_2T_x$-CoBDC measured at a potential of 1.64 V vs RHE (Inset: Equivalent circuit used to fit the Nyquist plots). (p) Stability test of $Ti_3C_2T_x$-CoBDC-based electrode in comparison with the standard IrO_2-based electrode, working at a constant potential of 1.64 V vs RHE for 10 000 s[56]. Copyright 2017, American Chemical Society.

markable HER performance with an overpotential of 49 mV at a current density of 10 mA/cm^2.

4.2. Supercapacitor

In order to find the solution to improve energy density, MOFs combining with electroactive materials of high pseudocapacitance have received wide attention, and the composites can realize synergetic effect of multi-functionalities. Based on different charging/discharging mechanism, MOFs with other function components have been used to acquire efficient supercapacitors. Typical MOF-based composites for supercapacitor are summarized in Table 5.

The introduction of conductive polymer is a choice to improve supercapacitor performance due to their low cost, high electrical conductivity and satisfactory specific capacitance[58–63]. Reversible redox reaction of doping and de-doping on the conductive polymer main chain not only increases the charge transport between MOFs by effectively linking up the isolated MOF particles and forming an "MOF to polymer to MOF" conducting pathway, but also provides extra capacitance. Fig. 5(a) exhibited an effective strategy to reduce the bulk electric resistance of MOFs by interweaving MOF crystals with polyaniline (PANI) chains that are electrochemically deposited on MOFs[58]. It was noteworthy that the PANI-ZIF-67 exhibited areal capacitance of 2146 mF/cm^2 at 10 mV/s (Figs. 5(b)–5(d)). Additionally, the hybrid architecture of Cu-MOF (Cu-CAT-NWAs) nanowire arrays on self-supported polypyrrole (PPy) membrane was reported for flexible supercapacitor electrodes by Hou and colleagues[63]. Preparation illustration of Cu-CAT-NWAs/PPy is shown in Fig. 5(e). The Cu-MOF nanowire arrays afforded high conductivity and sufficient active surface area for the accessibility of electrolyte, whereas the PPy membrane provided efficient charge transfer skeleton and extra capacitance. It significantly optimized the capacitive performance (Figs. 5(f)–(h)).

Additionally, introducing transition metal compounds

Table 5. The component of the MOF-based compositions for supercapacitor.

	Material	MOF	Function species	Ref.
1	PANI-ZIF-67	ZIF-67	PANI	[58]
2	Zn-MOF/PANI	Zn-MOF	PANI	[59]
3	Zn/Ni-MOF@PPy	Zn/Ni-MOF	PPy	[60]
4	ZIF@PPy	ZIF	PPy	[61]
5	NENU-5/PPy	NENU-5	PPy	[62]
6	Cu-MOF@PPy	Cu-MOF	PPy	[63]
7	MnO_x-MHCF	MHCF(Mn)	MnO_x	[64]
8	MoS_2@Ni-MOF	Ni-MOF	MoS_2	[65]

onto the surface of MOFs can also optimize active sites by modulating the surrounding chemical environment of MOF surface to promote surface redox reactions[64, 65]. The formed composite structure can not only accelerate the surface electrochemical adsorption to boost redox reaction, but also directly provide more active sites to enhance the energy density and power capability. MnO_x-MHCF was a typical example for supercapacitor to develop an in-situ self-transformation method[64]. The results indicated that MnO_x-MHCF displayed threefold increase in capacitance (an areal capacitance of 175 mF/cm^2 at 0.5 mA/cm^2) and superior rate performance, including as shown in Figs. 5(j)–5(l). MnO_x-MHCF electrode retained more than 94.7% of its initial capacitance after 10 000 cycles at 10 A/g as shown in Fig. 5(m). The highly efficient supercapacitor performance of the composites was attributed to more intimate connection between MnO_x and MOFs and resulting fast surface redox reaction. Besides, Yue and co-workers reported a hydrothermal intercalation self-assembly method to coat Ni-MOF on the spherical nanoflower MoS_2[65]. The introduced non-metal S could join different metal ions to form a new interface. And the formed structure would facilitate charge storage. The MoS_2@Ni-MOF exhibited a specific capacitance of 1590.24 F/g at a current density of 1.0 A/g and a cycle stability (retention rate of 87.97% after 20 000 cycles at current of 5.0 A/g).

4.3. Ion battery

Integrating electrochemically active components within MOFs can directly enhance the capacity by taking the contributions of other function components. Each component within the composites serves simultaneously as function components and further achieves the synergy because of the strong interconnection among these components[18, 66]. Typical MOF-based composites as electrodes and separators of ion battery are summarized in Table 6.

Electrodes materials are the key and core constituents within ion battery[67–69]. The MOF-based materials with other function components can provide abundant redox-active sites and enhance the electronic conductivity to ensure high ions storage capability. Both of MOFs and other function components can provide capacity for energy storage. It should be stated that extra capability can also be provided due to the strong interconnection among these components or the interfaces between these components. On one hand, enhanced rate capability can be realized via smaller electrochemical resistance due to formation of interfaces between different function components. And it decreased the distance for ions migration and storage. On the other hand, introducing active materials can reduce the pulverization and agglomeration of MOFs to improve structural stability. As shown in Fig. 6(a), the CuS@Cu-BTC was designed as the anode of lithium-ion batteries by Wang and colleagues[67]. This composite showed a high capacity (1609 mAh/g at 100 mA/g) and 490 mAh/g at 1000 mA/g (Figs. 6(b)–6(d)). The work achieved the synergistic effects based on the advantages of robust structure interconnected between CuS and Cu-BTC, which could provide extra ion storage capacity. On the one hand, Cu-BTC not only ensured the porosity to improve ions storage and electrolyte diffusion, but also provided substrates to accommodate the volume change of CuS and stress relaxation of electrodes. On the other hand, the in-situ fabrication of CuS on the Cu-BTC contributed to minimize electrochemical resistance. And it shortened the diffusion path of ions and electrons. The synergistic effect was also observed in few-layer black phosphorus (BP) decorated NiCo-MOF nanosheets as anode material for battery[68]. In the composites, the NiCo-MOF increased contact areas between electrode and electrolyte. The BP could increase electronic conductivity to provide favorable pathways for charge transport. And 2D layer nanostructure of composites provided sufficient space to buffer the volume change during cycling due to the thermodynamic stability of BP. As a result, the work displayed a reversible capacity of 853 mAh/g at 0.5 A/g. It also showed long cycle life and high rate capability of 398 mAh/g at 5 A/g after 1000 cycles. Additionally, the structure of MOFs suffered from gradual deterioration after long-term cycling as a cathode for Li–S battery, and they were unable to retain soluble polysulfides. It inevitably limits their practical applications for energy storage. Baumann and co-workers[69] utilized Li_3PS_4 within the Zr-MOF (noted as LPS-UiO-66) for lithium–sulfur batteries as shown in Fig. 6(e). The work indicated that lithium phosphorus sulfide encapsulated in MOFs could decrease the harmful dissolution of polysulfides and thiophosphate into the electrolyte. It could be attributed to the reversible formation of S–S bonds between lithium phosphorus sulfide and solubilized polysulfides based on the combination of Li_3PS_4 and Zr-MOF. The formation of S–S bonds could enhance polysulfide encapsulation to improve stability. As a result, it gained a sustainable high capacity over prolonged cycling for reasons that the composites could boost conversion of polysulfides and ensure sulfur utilization at high sulfur loading (Figs. 6(f)–6(h)).

For composite separators, MOFs suffered from gradual deterioration and was unable to retain soluble polysulfides after long-term cycling[70–72]. Loading MOFs on carbon materials can develop functional separators. The separators not only enhance the reaction kinetics process to boost the conversion of polysulfides, but also greatly decreased their interfacial resistance to gain the high conductivity derived from carbon materials. And carbon materials can also directly participate in the process of blocking the polysulfide shuttle. Hong and co-workers[72] proposed Ce-MOF/CNT composites as separator coating materials in the Li–S battery system as shown in Fig. 6(i). Due to the existence of CNTs, the composites could improve the surface reaction kinetics via transforming polysulfides into short chain lithium sulfides to reduce the shuttle of polysulfides. And this study indicated that CNT could act as secondary charge collector to promote electric conduction. It was noteworthy that the initial specific capacity of the cell with Ce-MOF-2/CNT coating was as high as

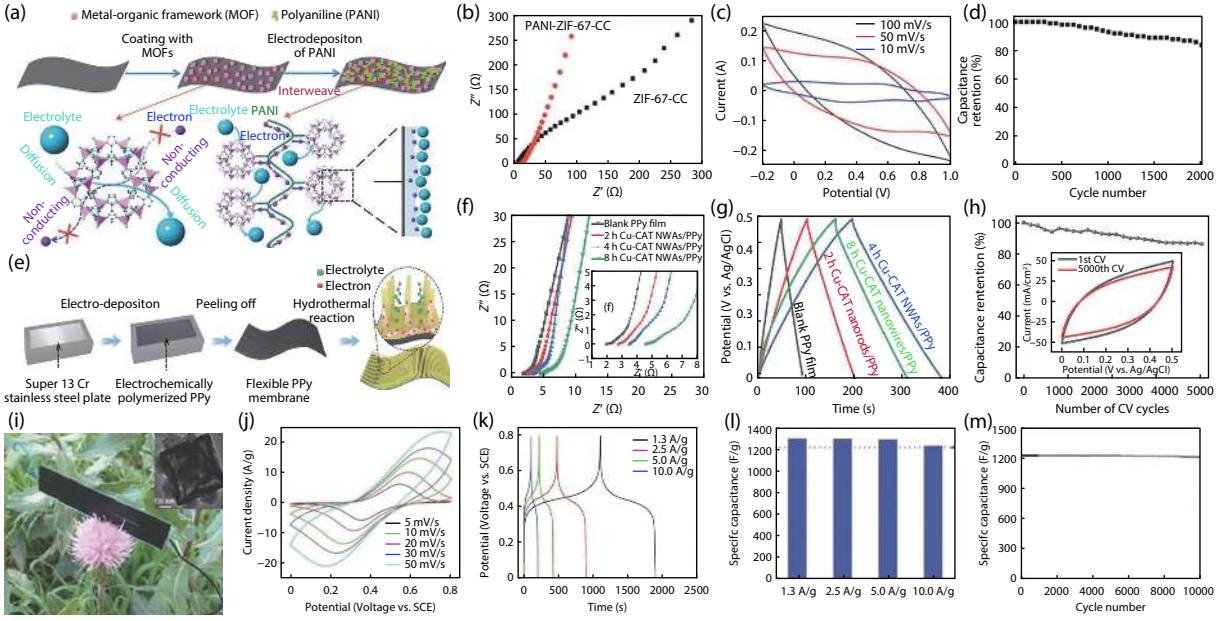

Fig. 5. (Color online) Typical examples of MOFs with function components for catalysis. (a) Schematic illustration of PANI-ZIF-67. (b) Nyquist electrochemical impedance spectra of ZIF-67-CC and PANI-ZIF-67-CC. (c) Cyclic voltammograms collected of PANI-ZIF-67-CC electrode at different scan rate in 3 M KCl. (d) Cycling performance of the solid-state SC device measured at 0.1 mA/cm^2 for 2000 cycles[58]. Copyright 2019, American Chemical Society. (e) Preparation illustration of Cu-CAT-NWAs/PPy. (f) Nyquist electrochemical impedance spectra of pristine PPy and various time-dependent Cu-CAT-NWAs/PPy based electrodes. (g) The galvanostatic charge-discharge curves at different current densities of Cu-CAT-NWAs/PPy electrode. (h) Cyclic stability over 5000 cycles under a scan rate of 100 mV/s for Cu-CAT-NWAs/PPy electrode[63]. Copyright 2020, Wiley-VCH Verlag GmbH & Co. KGaA. (i) Photographs of the solidstate SC device (inset: SEM image of MnO_x-MHCF). (j) Cyclic voltammogram curves of MnO_x-MHCF electrode at different scan rates in the range of 5–50 mV/s. (k) The galvanostatic charge-discharge curves of MnO_x-MHCF electrode at current densities of 1.3–10.0 A/g. (l) Specific capacitances of MnO_x-MHCF nanocube electrodes derived from the discharging curves at the current density of 1.3–10.0 A/g. (m) Cycling performance of the MnOx-MHCF nanocube electrode measured at the current density of 10.0 A/g for 10 000 cycles[64]. Copyright 2016, Wiley-VCH Verlag GmbH & Co. KGaA.

Table 6. The component of the MOF-based compositions for battery.

	Material	MOF	Function species	Application	Ref.
1	CuFe-PBA@ NiFe-PBA	CuFe-PBA	NiFe-PBA	Cathode	[18]
2	CuS@Cu-BTC	Cu-BTC	CuS	Anode	[67]
3	BP/NiCo-MOF	NiCo-MOF	BP	Anode	[68]
4	Li_3PS_4-Zr-MOF	Zr-MOF	Li_3PS_4	Cathode	[69]
5	HKUST-1@GO	HKUST-1	GO	Separator	[71]
6	Ce-MOF/CNT	Ce-MOF	CNT	Separator	[72]

1021.8 mAh/g, which was reduced to 838.8 mAh/g after 800 cycles with a decay rate of 0.022%, and the Coulombic efficiency was nearly 100% (Figs. 6(j)–6(l)).

5. Summary and perspective

MOFs exhibit impressive physicochemical properties and unique fancy owing to diversity of the organic linkers and the metal nodes, regular and tunable pore structure, and chemical tunability. Hence, MOF-based composites have attracted intensive attention and yielded excellent performance for energy conversion and storage. In this review, we have summarized recent progress and typical development strategies of MOF-based composites for energy conversion and storage such as catalysis, supercapacitor, and ion battery. Moreover, we present the design principle from the viewpoint of the intrinsic relationships among different components and properties of energy conversion and storage, including two working modes: MOFs with assistant the components and MOFs with other function components. For 'MOFs with assistant the components' mode, MOFs possess the main function in the composites, while the other components will not directly participate the energy conversion and storage, but can assist MOFs for full utilizations by adjusting related properties; For 'MOFs with other function components' mode, all MOFs and the other components join energy conversion and storage simultaneously.

Despite these great achievements, there are still some foreseeable challenges in large-scale applications. (1) Although the addition of conductive materials can mitigate the impacts of poor electrical conductivity, the overall resistance of MOF-based composites is still high. Adjusting ligands of MOFs endow tunable electronic structure to overcome this drawback. Similarly, combining molecular design within composites will contribute more possibilities to optimizing the final energy conversion and storage. (2) The precise control of composite proportion and coordination environment is another inevitable challenge. Direct insight into targeted active sites in practical applications is still undefined, which is significant to push further fundamental understandings towards synergies among different components in the MOF-based composites.

Recently, rational compositional design of MOF-derived materials based on judicious selection of MOF precursors and controlled thermal/chemical conversion processes has also drawn great attention[73–75]. MOFs or MOF composites are

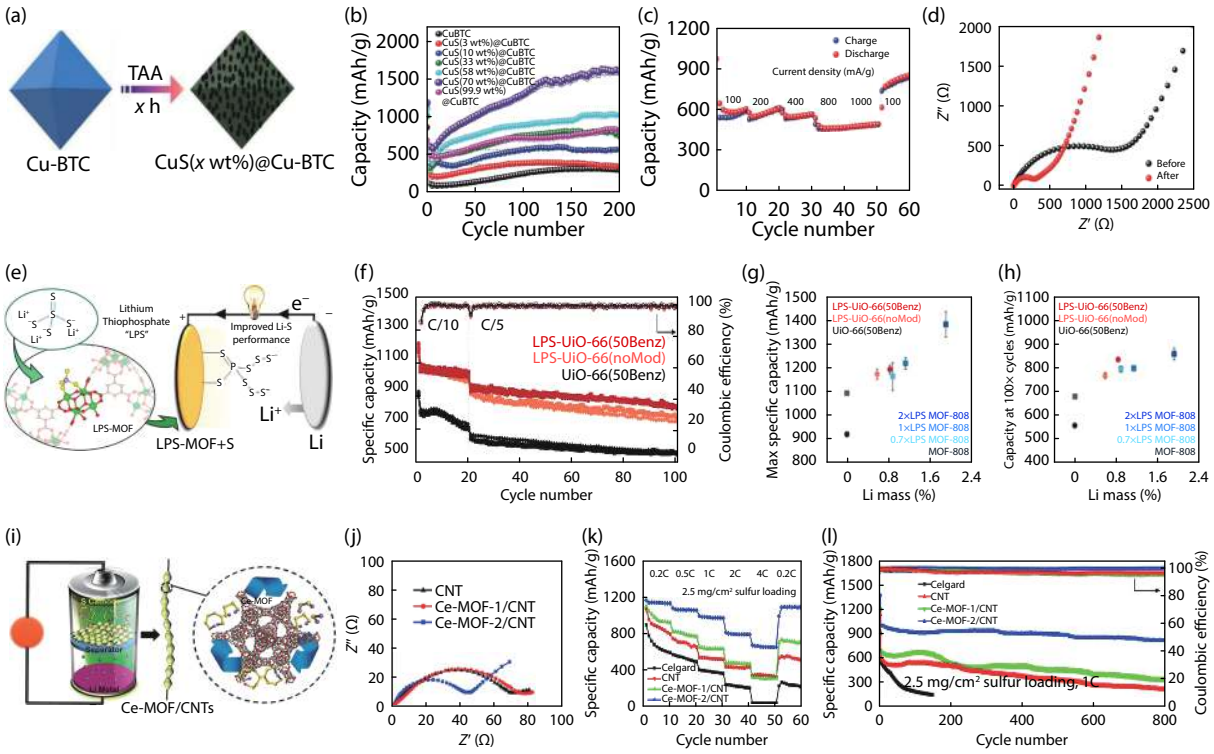

Fig. 6. (Color online) Typical examples of MOFs with function components for catalysis. (a) Schematic illustration of the synthetic process of CuS (*x* wt%)@Cu-BTC composites. (b) Cycling performance of Cu-BTC and the composites. (c) Rate capabilities and (d) impedance spectrum of CuS (70 wt%)@Cu-BTC[67]. Copyright 2019, Wiley-VCH Verlag GmbH & Co. KGaA. (e) Schematic illustration of LPS-UiO-66. (f) Cycling performance of LPS-UiO-66-containing cells. (g) Maximum capacity and (h) capacity after 100 cycles for various MOF composite cells[69]. Copyright 2019, American Chemical Society. (i) Scheme of MOFs/CNT composites with catalysis of the conversion of polysulfides as the separator coating materials for Li–S battery. (j) Impedance spectrum of symmetrical cells using different coating materials of CNT, Ce-MOF-1/CNT, and Ce-MOF-2/CNT. (k) Rate performance at various C-rates for the different separators. (l) Cyclic performance of cells with different separators at 1 C for 800 cycles[72]. Copyright 2019, American Chemical Society.

used as sacrificial templates to design various nanomaterials, which can form new active sites or improve electrochemical performance. The metal nodes in MOFs can be converted into metal nanoparticles or metal compounds, and the organic linkers are transformed into porous carbon materials or removed[75]. The rational design and in-situ synthesis of hierarchical porous composites could improve the availability of active sites, mass transport, and gas release. However, some key problems still exist for practical applications. For example, the complexity of MOF-derived composites makes the identification and optimization of true active sites difficult. And the high surface area and porosity of MOF-derived composites may lead to low initial Coulombic efficiency and low tap density.

Although there are still many challenges, it is believed that more progresses of MOF-based composites, based on the above design principle of two working modes, will be expected to maximize composite performance for energy conversion and storage in the near years. In addition, the MOF-based composites are encouraged to gain more achievement in new energy-related fields. Hence, this review aims to provide general design principle to further applications of MOF-based composites for energy conversion and storage. We keep looking forward to the beautiful future of MOF.

Acknowledgements

The authors gratefully acknowledge the financial support from the National Natural Science Foundation of China (NNSFC grants 21707093).

References

[1] Dhakshinamoorthy A, Asiri A M, García H. Metal-organic framework (MOF) compounds: Photocatalysts for redox reactions and solar fuel production. Angew Chem Int Ed, 2016, 55(18), 5414

[2] Zheng S, Li X, Yan B, et al. Transition-metal (Fe, Co, Ni) based metal-organic frameworks for electrochemical energy storage. Adv Energy Mater, 2017, 7(18), 1602733

[3] Liang Z, Qu C, Guo W, et al. Pristine metal-organic frameworks and their composites for energy storage and conversion. Adv Mater, 2018, 30(37), 1702891

[4] Dong R, Han P, Arora H, et al. High-mobility band-like charge transport in a semiconducting two-dimensional metal-organic framework. Nat Mater, 2018, 17(11), 1027

[5] Song Y, Li Z, Zhu Y, et al. Titanium hydroxide secondary building units in metal-organic frameworks catalyze hydrogen evolution under visible light. J Am Chem Soc, 2019, 141(31), 12219

[6] Sheberla D, Bachman J C, Elias J S, et al. Conductive MOF electrodes for stable supercapacitors with high areal capacitance. Nat Mater, 2017, 16(2), 220

[7] Lee J H, Ali G, Kim D H, et al. Metal-organic framework cathodes based on a vanadium hexacyanoferrate prussian blue analogue for high-performance aqueous rechargeable batteries. Adv Energy Mater, 2017, 7(2), 1601491

[8] Wilmer C E, Leaf M, Lee C Y, et al. Large-scale screening of hypothetical metal-organic frameworks. Nat Chem, 2012, 4(2), 83

[9] Falcaro P, Okada K, Hara T, et al. Centimetre-scale micropore alignment in oriented polycrystalline metal-organic framework films via heteroepitaxial growth. Nat Mater, 2017, 16(3), 342
[10] Zhu Y, Ciston J, Zheng B, et al. Unravelling surface and interfacial structures of a metal-organic framework by transmission electron microscopy. Nat Mater, 2017, 16(5), 532
[11] Liu G, Chernikova V, Liu Y, et al. Mixed matrix formulations with MOF molecular sieving for key energy-intensive separations. Nat Mater, 2018, 17(3), 283
[12] Van Wyk A, Smith T, Park J, et al. Charge-transfer within Zr-based metal-organic framework: The role of polar node. J Am Chem Soc, 2018, 140(8), 2756
[13] Feng D, Lei T, Lukatskaya M R, et al. Robust and conductive two-dimensional metal-organic frameworks with exceptionally high volumetric and areal capacitance. Nat Energy, 2018, 3(1), 30
[14] Jiang Q, Xiong P, Liu J, et al. A redox-active 2D metal-organic framework for efficient lithium storage with extraordinary high capacity. Angew Chem Int Ed, 2020, 59(13), 5273
[15] Yuan Y P, Yin L S, Cao S W, et al. Improving photocatalytic hydrogen production of metal-organic framework UiO-66 octahedrons by dye-sensitization. Appl Catal B, 2015, 168/169, 572
[16] Wu D, Guo Z, Yin X, et al. Metal-organic frameworks as cathode materials for Li-O_2 batteries. Adv Mater, 2014, 26(20), 3258
[17] Chen Y Z, Wang Z U, Wang H, et al. Singlet oxygen-engaged selective photo-oxidation over pt nanocrystals/porphyrinic MOF: The roles of photothermal effect and pt electronic state. J Am Chem Soc, 2017, 139(5), 2035
[18] Asakura D, Li C H, Mizuno Y, et al. Bimetallic cyanide-bridged coordination polymers as lithium ion cathode materials: core@shell nanoparticles with enhanced cyclability. J Am Chem Soc, 2013, 135(7), 2793
[19] Zhong H, Ghorbani-Asl M, Ly K H, et al. Synergistic electroreduction of carbon dioxide to carbon monoxide on bimetallic layered conjugated metal-organic frameworks. Nat Commun, 2020, 11(1), 1409
[20] Zhu Y P, Yin J, Abou-Hamad E, et al. Highly stable phosphonate-based MOFs with engineered bandgaps for efficient photocatalytic hydrogen production. Adv Mater, 2020, 32(16), 1906368
[21] Li Q, Fan Z L, Xue D X, et al. A multi-dye@MOF composite boosts highly efficient photodegradation of an ultra-stubborn dye reactive blue 21 under visible-light irradiation. J Mater Chem A, 2018, 6(5), 2148
[22] Li M, Zheng Z, Zheng Y, et al. Controlled growth of metal-organic framework on upconversion nanocrystals for NIR-enhanced photocatalysis. ACS Appl Mater Interfaces, 2017, 9(3), 2899
[23] Liu N, Huang W, Zhang X, et al. Ultrathin graphene oxide encapsulated in uniform MIL-88A(Fe) for enhanced visible light-driven photodegradation of RhB. Appl Catal B, 2018, 221, 119
[24] Li S, Ji K, Zhang M, et al. Boosting photocatalytic CO_2 reduction of metal-organic frameworks by encapsulating carbon dots. Nanoscale, 2020, 12(17), 9533
[25] Jahan M, Bao Q, Loh K P. Electrocatalytically active graphene-porphyrin MOF composite for oxygen reduction reaction. J Am Chem Soc, 2012, 134(15), 6707
[26] Fang Y, Li X, Li F, et al. Self-assembly of cobalt-centered metal organic framework and multiwalled carbon nanotubes hybrids as a highly active and corrosion-resistant bifunctional oxygen catalyst. J Power Sources, 2016, 326, 50
[27] Xiong W, Li H, You H, et al. Encapsulating metal organic framework into hollow mesoporous carbon sphere as efficient oxygen bifunctional electrocatalyst. Natl Sci Rev, 2019, 7(3), 609
[28] Xu C, Pan Y, Wan G, et al. Turning on visible-light photocatalytic C-H oxidation over metal-organic frameworks by introducing metal-to-cluster charge transfer. J Am Chem Soc, 2019, 141(48), 19110
[29] Zhang W, Wang Y, Zheng H, et al. Embedding ultrafine metal oxide nanoparticles in monolayered metal-organic framework nanosheets enables efficient electrocatalytic oxygen evolution. ACS Nano, 2020, 14(2), 1971
[30] Zhang H, Wei J, Dong J, et al. Efficient visible-light-driven carbon dioxide reduction by a single-atom implanted metal-organic framework. Angew Chem Int Ed, 2016, 55(46), 14310
[31] Bi S, Banda H, Chen M, et al. Molecular understanding of charge storage and charging dynamics in supercapacitors with MOF electrodes and ionic liquid electrolytes. Nat Mater, 2020, 19(5), 552
[32] Skorupskii G, Trump B A, Kasel T W, et al. Efficient and tunable one-dimensional charge transport in layered lanthanide metal-organic frameworks. Nat Chem, 2020, 12(2), 131
[33] Rajak R, Saraf M, Mobin S M. Robust heterostructures of a bimetallic sodium-zinc metal-organic framework and reduced graphene oxide for high-performance supercapacitors. J Mater Chem A, 2019, 7(4), 1725
[34] Zhou Y, Mao Z, Wang W, et al. In-situ fabrication of graphene oxide hybrid ni-based metal-organic framework (Ni-MOFs@GO) with ultrahigh capacitance as electrochemical pseudocapacitor materials. ACS Appl Mater Interfaces, 2016, 8(42), 28904
[35] Wen P, Gong P, Sun J, et al. Design and synthesis of Ni-MOF/CNT composites and rGO/carbon nitride composites for an asymmetric supercapacitor with high energy and power density. J Mater Chem A, 2015, 3(26), 13874
[36] Deng T, Lu Y, Zhang W, et al. Inverted design for high-performance supercapacitor via $Co(OH)_2$-derived highly oriented MOF electrodes. Adv Energy Mater, 2018, 8(7), 1702294
[37] Zhou S, Kong X, Zheng B, et al. Cellulose nanofiber @ conductive metal-organic frameworks for high-performance flexible supercapacitors. ACS Nano, 2019, 13(8), 9578
[38] Tian D, Song N, Zhong M, et al. Bimetallic MOF nanosheets decorated on electrospun nanofibers for high-performance asymmetric supercapacitors. ACS Appl Mater Interfaces, 2020, 12(1), 1280
[39] Jiang H, Liu X C, Wu Y, et al. Metal-organic frameworks for high charge-discharge rates in lithium-sulfur batteries. Angew Chem Int Ed, 2018, 57(15), 3916
[40] Gao C, Wang P, Wang Z, et al. The disordering-enhanced performances of the Al-MOF/graphene composite anodes for lithium ion batteries. Nano Energy, 2019, 65, 104032
[41] Wei T, Zhang M, Wu P, et al. POM-based metal-organic framework/reduced graphene oxide nanocomposites with hybrid behavior of battery-supercapacitor for superior lithium storage. Nano Energy, 2017, 34, 205
[42] Hou Y, Mao H, Xu L. MIL-100(V) and MIL-100(V)/rGO with various valence states of vanadium ions as sulfur cathode hosts for lithium-sulfur batteries. Nano Res, 2017, 10(1), 344
[43] Mao Y, Li G, Guo Y, et al. Foldable interpenetrated metal-organic frameworks/carbon nanotubes thin film for lithium-sulfur batteries. Nat Commun, 2017, 8(1), 14628
[44] Zhang H, Zhao W, Zou M, et al. 3D, mutually embedded MOF@carbon nanotube hybrid networks for high-performance lithium-sulfur batteries. Adv Energy Mater, 2018, 8(19), 1800013
[45] Zang Y, Pei F, Huang J, et al. Large-area preparation of crack-free crystalline microporous conductive membrane to upgrade high energy lithium-sulfur batteries. Adv Energy Mater, 2018, 8(31), 1802052
[46] He Y, Chang Z, Wu S, et al. simultaneously inhibiting lithium dendrites growth and polysulfides shuttle by a flexible MOF-based membrane in Li–S batteries. Adv Energy Mater, 2018, 8(34), 1802130
[47] Zhang C, Shen L, Shen J, et al. Anion-sorbent composite separators for high-rate lithium-ion batteries. Adv Mater, 2019, 31(21), 1808338
[48] Zhang F M, Sheng J L, Yang Z D, et al. Rational design of MOF/COF hybrid materials for photocatalytic H_2 evolution in the presence of sacrificial electron donors. Angew Chem Int Ed, 2018,

57(37), 12106
[49] Ran J, Qu J, Zhang H, et al. 2D metal organic framework nanosheet: A universal platform promoting highly efficient visible-light-induced hydrogen production. Adv Energy Mater, 2019, 9(11), 1803402
[50] Shi L, Wang T, Zhang H, et al. Electrostatic self-assembly of nanosized carbon nitride nanosheet onto a zirconium metal-organic framework for enhanced photocatalytic CO_2 reduction. Adv Funct Mater, 2015, 25(33), 5360
[51] Kong Z C, Liao J F, Dong Y J, et al. Core@shell $CsPbBr_3$@zeolitic imidazolate framework nanocomposite for efficient photocatalytic CO_2 reduction. ACS Energy Lett, 2018, 3(11), 2656
[52] Wu L Y, Mu Y F, Guo X X, et al. encapsulating perovskite quantum dots in iron-based metal-organic frameworks (MOFs) for efficient photocatalytic CO_2 reduction. Angew Chem Int Ed, 2019, 58(28), 9491
[53] Fang X, Shang Q, Wang Y, et al. Single Pt atoms confined into a metal-organic framework for efficient photocatalysis. Adv Mater, 2018, 30(7), 1705112
[54] Xia Z, Fang J, Zhang X, et al. Pt nanoparticles embedded metal-organic framework nanosheets: A synergistic strategy towards bifunctional oxygen electrocatalysis. Appl Catal B, 2019, 245, 389
[55] Rui K, Zhao G, Lao M, et al. Direct hybridization of noble metal nanostructures on 2D metal-organic framework nanosheets to catalyze hydrogen evolution. Nano Lett, 2019, 19(12), 8447
[56] Zhao L, Dong B, Li S, et al. Interdiffusion reaction-assisted hybridization of two-dimensional metal-organic frameworks and $Ti_3C_2T_x$ nanosheets for electrocatalytic oxygen evolution. ACS Nano, 2017, 11(6), 5800
[57] Liu T, Li P, Yao N, et al. CoP-doped MOF-based electrocatalyst for pH-universal hydrogen evolution reaction. Angew Chem Int Ed, 2019, 58(14), 4679
[58] Wang L, Feng X, Ren L, et al. Flexible solid-state supercapacitor based on a metal-organic framework interwoven by electrochemically-deposited PANI. J Am Chem Soc, 2015, 137(15), 4920
[59] Guo S, Zhu Y, Yan Y, et al. (Metal-organic framework)-polyaniline sandwich structure composites as novel hybrid electrode materials for high-performance supercapacitor. J Power Sources, 2016, 316, 176
[60] Jiao Y, Chen G, Chen D, et al. Bimetal-organic framework assisted polymerization of pyrrole involving air oxidant to prepare composite electrodes for portable energy storage. J Mater Chem A, 2017, 5(45), 23744
[61] Xu X, Tang J, Qian H, et al. Three-dimensional networked metal-organic frameworks with conductive polypyrrole tubes for flexible supercapacitors. ACS Appl Mater Interfaces, 2017, 9(44), 38737
[62] Wang H N, Zhang M, Zhang A M, et al. Polyoxometalate-based metal-organic frameworks with conductive polypyrrole for supercapacitors. ACS Appl Mater Interfaces, 2018, 10(38), 32265
[63] Hou R, Miao M, Wang Q, et al. Integrated conductive hybrid architecture of metal-organic framework nanowire array on polypyrrole membrane for all-solid-state flexible supercapacitors. Adv Energy Mater, 2020, 10(1), 1901892
[64] Zhang Y Z, Cheng T, Wang Y, et al. A simple approach to boost capacitance: Flexible supercapacitors based on manganese oxides@MOFs via chemically induced in situ self-transformation. Adv Mater, 2016, 28(26), 5242
[65] Yue L, Wang X, Sun T, et al. Ni-MOF coating MoS_2 structures by hydrothermal intercalation as high-performance electrodes for asymmetric supercapacitors. Chem Eng J, 2019, 375, 121959
[66] Zhang Z, Yoshikawa H, Awaga K. Monitoring the solid-state electrochemistry of Cu(2,7-AQDC) (AQDC = anthraquinone dicarboxylate) in a lithium battery: Coexistence of metal and ligand redox activities in a metal-organic framework. J Am Chem Soc, 2014, 136(46), 16112
[67] Wang P, Shen M, Zhou H, et al. MOF-derived CuS@Cu-BTC composites as high-performance anodes for lithium-ion batteries. Small, 2019, 15(47), 1903522
[68] Jin J, Zheng Y, Huang S Z, et al. Directly anchoring 2D NiCo metal-organic frameworks on few-layer black phosphorus for advanced lithium-ion batteries. J Mater Chem A, 2019, 7(2), 783
[69] Baumann A E, Han X, Butala M M, et al. Lithium thiophosphate functionalized zirconium MOFs for Li–S batteries with enhanced rate capabilities. J Am Chem Soc, 2019, 141(44), 17891
[70] Li Y, Lin S, Wang D, et al. Single atom array mimic on ultrathin MOF nanosheets boosts the safety and life of lithium-sulfur batteries. Adv Mater, 2020, 32(8), 1906722
[71] Bai S, Liu X, Zhu K, et al. Metal-organic framework-based separator for lithium-sulfur batteries. Nat Energy, 2016, 1(7), 16094
[72] Hong X J, Song C L, Yang Y, et al. Cerium based metal-organic frameworks as an efficient separator coating catalyzing the conversion of polysulfides for high performance lithium-sulfur batteries. ACS Nano, 2019, 13(2), 1923
[73] Chen W, Pei J, He C T, et al. Single tungsten atoms supported on MOF-derived N-doped carbon for robust electrochemical hydrogen evolution. Adv Mater, 2018, 30(30), 1800396
[74] Wang Q, Luo Y, Hou R, et al. Redox tuning in crystalline and electronic structure of bimetal-organic frameworks derived cobalt/nickel boride/sulfide for boosted faradaic capacitance. Adv Mater, 2019, 31(51), 1905744
[75] Wang Z, Shen J, Liu J, et al. Self-supported and flexible sulfur cathode enabled via synergistic confinement for high-energy-density lithium-sulfur batteries. Adv Mater, 2019, 31(33), 1902228